European Commission

JRC TECHNICAL REPORTS

Characterisation of plastic scintillators used as an active background shield for neutron detection

Exploratory research project IntelligentShield, deliverable 10

Jan Paepen
Fabian Schulte
Pierfrancesco Mastinu
Bent Pedersen
Holger Saare
Peter Schillebeeckx
Alan Tkaczyk
Giovanni Varasano

2016

Joint Research Centre

EUR 27930 EN

JRC Science Hub
https://ec.europa.eu/jrc

JRC101510

EUR 27930 EN

ISBN 978-92-79-58436-7 (PDF)

ISSN 1831-9424 (online)

doi: 10.2787/810820 (online)

How to cite: J. Paepen, F. Schulte, P. Mastinu B. Pedersen, H. Saare, P. Schillebeeckx, A. Tkaczyk and G. Varasano; Characterisation of plastic scintillators used as an active background shield for neutron detection; EUR 27930 EN; doi: 10.2787/810820

Characterisation of plastic scintillators used as an active background shield for neutron detection

J. Paepen[a], F. Schulte[b], P. Mastinu[c] B. Pedersen[d], H. Saare[e], P. Schillebeeckx[a], A. Tkaczyk[e] and G. Varasano[d]

[a]European Commission, Joint Research Centre, B - 2440 Geel, Belgium

[b]Fachhochschule Aachen, University of Applied Sciences, G - 52005 Aachen, Germany

[c]INFN, Laboratori Nazionali di Legnaro, I-35020 Legnaro, Italy

[d]European Commission, Joint Research Centre, I – 21020 Ispra, Italy

[e]University of Tartu, Institute of Physics, EE – 50411 Tartu, Estonia

Contents

Abstract

This work is part of a JRC Exploratory Research project to develop an active shield that is used to reduce the background due to cosmic radiation in a low-level nuclear waste detection system. The shield consists of an array of plastic scintillators surrounding the detection system.

Commercially available plastic scintillation detectors with different thicknesses were characterized for their response to gamma rays, neutrons and muons. Response functions to gamma rays were determined by measurements with radionuclide sources in the energy range from 0.6 MeV to 6.0 MeV. Neutron response functions were measured at mono-energetic neutron beams produced at the Van de Graaff accelerator of the JRC Geel (B) and were derived from results of time-of-flight measurements at the Van de Graaff accelerator of the INFN Legnaro (I). From the response functions for gamma rays and neutrons, light output and resolution functions for protons and electrons were derived.

Experimental response functions for muons were determined with the detectors positioned at different orientations. The muon peak is more pronounced in horizontally oriented detectors. Using a scintillator with a minimum thickness of 20 mm a signal caused by the detection of a muon can be separated from events due to natural gamma ray background.

For detectors that are stacked, signals caused by the detection of muons can be identified based on a coincidence pattern. Hence, requirements on such a coincidence pattern together with requirements on the light production are effective as parameters for the veto system to be designed.

1 Introduction

Non-destructive methods to characterize α-active nuclear waste strongly rely on the detection of neutrons. Neutron emission by α-active waste is caused by spontaneous fission, (α,n) reactions on light nuclei and multiplication of neutrons by neutron induced fission reactions. When nuclear fission occurs a group of prompt fission neutrons is emitted simultaneously. These neutrons have an energy distribution, which in first approximation follows a Maxwellian distribution with an average energy in the order of 2 MeV. The number of emitted prompt fission neutrons, often referred to as multiplicity, is characterised by a statistical distribution. In an (α,n) reaction only one neutron is emitted. The difference between the neutron multiplicity of neutrons resulting from fission and an (α,n) reaction can be used to distinguish between them.

Waste characterisation systems consist mostly of a moderator surrounding a neutron detector that is sensitive to low energy neutrons, in most cases a proportional counter filled with ^{3}He gas. The detection system is connected to a signal processer that allows a multiplicity analysis of neutrons that are correlated in time. The pioneering work of such an analysis has been carried out by Hage and Cifarelli at JRC Ispra (I) [1], [2], [3]. They developed analytical expressions to link the total spontaneous fission rate, the ratio of (α,n) neutrons to spontaneous fission neutrons, the multiplication and detection efficiency to the experimental observables. The result of such a multiplicity or neutron correlation analysis can be used to determine the amount of Pu in a drum containing nuclear waste.

The data analysis can strongly be hampered when spallation reactions are induced in the waste and/or materials surrounding the detection system. Such spallation reactions can be induced by high-energetic atmospheric muons. They are followed by the emission of neutrons with a relatively high multiplicity. Hence, it is difficult to separate them from prompt fission neutrons. Since an increase of the amount of material around the detector would increase this contribution, passive shielding is not recommended. Therefore, an active shield is proposed that consists of an array of plastic scintillators surrounding the measurement setup. The idea is to inhibit the treatment of a signal observed in the neutron detector, once a muon enters the system from outside and is detected in the plastic scintillators. This concept of the JRC Exploratory Research project "IntelligentShield" is illustrated in Figure 1.

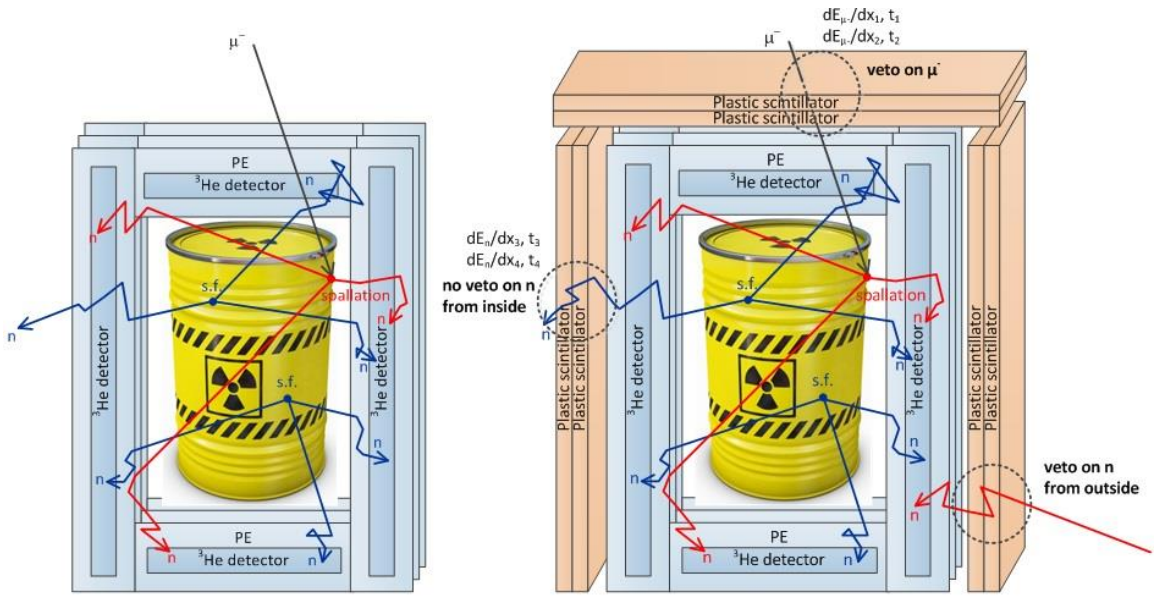

Figure 1. Schematic representation of a waste assay system based on neutron detection (left). A system surrounded by plastic scintillators is shown on the right. The scintillator detectors are used to inhibit the detection in the waste assay system when atmospheric muons or neutrons from outside the system are detected in the scintillators.

In this work the main characteristics of plastic scintillators to be used as veto detectors are studied. A set of commercially available EJ-200 plastic scintillators with different thicknesses were characterized for their response to gamma rays, neutrons and muons. Response functions for neutrons were obtained from experiments with mono-energetic neutrons at the Van de Graaff accelerator of the JRC at Geel (B) and time-of-flight measurements at the Van de Graaff accelerator of the INFN in Legnaro (I). The response to gamma rays and muons were determined at JRC Geel (B) by measurements with radionuclide sources and background measurements, respectively.

2 Properties of EJ-200 scintillators

The performances of six rectangular EJ-200 plastic scintillators with different thicknesses, purchased from SCIONIX, were investigated. Each scintillator has a length of 40 cm and a width of 30 cm. Of the six plastic scintillation detectors that were used, two have a thickness of 12.7 mm (serial numbers SFQ 537, SFQ 538), two of 20 mm (SFQ 539, SFQ 540) and two of 25 mm (SFQ 541, SFQ 542). Their characteristics are summarized in Table 1 [4]. A technical drawing of the SFQ 538 (12.7 mm) plastic scintillator is shown in Figure 2.

The scintillators were coupled to a cylindrical 51 mm diameter photomultiplier tube (PMT, ET Enterprises 9214B series) [5]. The technical specifications of such a PMT (9214B series) are listed in Table 2. The optimum operating voltage of the detector response for gamma ray sources was given by a test sheet from SCIONIX for each detector and was slightly adjusted for an easier analysis of the measurement results. Two signals were provided: one from the anode and one from the last dynode before the anode. The PMT was powered with a portable high voltage supply, FAST ComTec model SHQ 222M.

To match the rectangular shape of the scintillator with a circular PMT a light guide is needed. The light guides for the EJ-200 detectors were made out of polymethylmethacrylate (PMMA). Their properties are specified in Table 3 [6], [7].The scintillators and light guides used in this work were wrapped in black vinyl to prevent penetration of light from the environment.

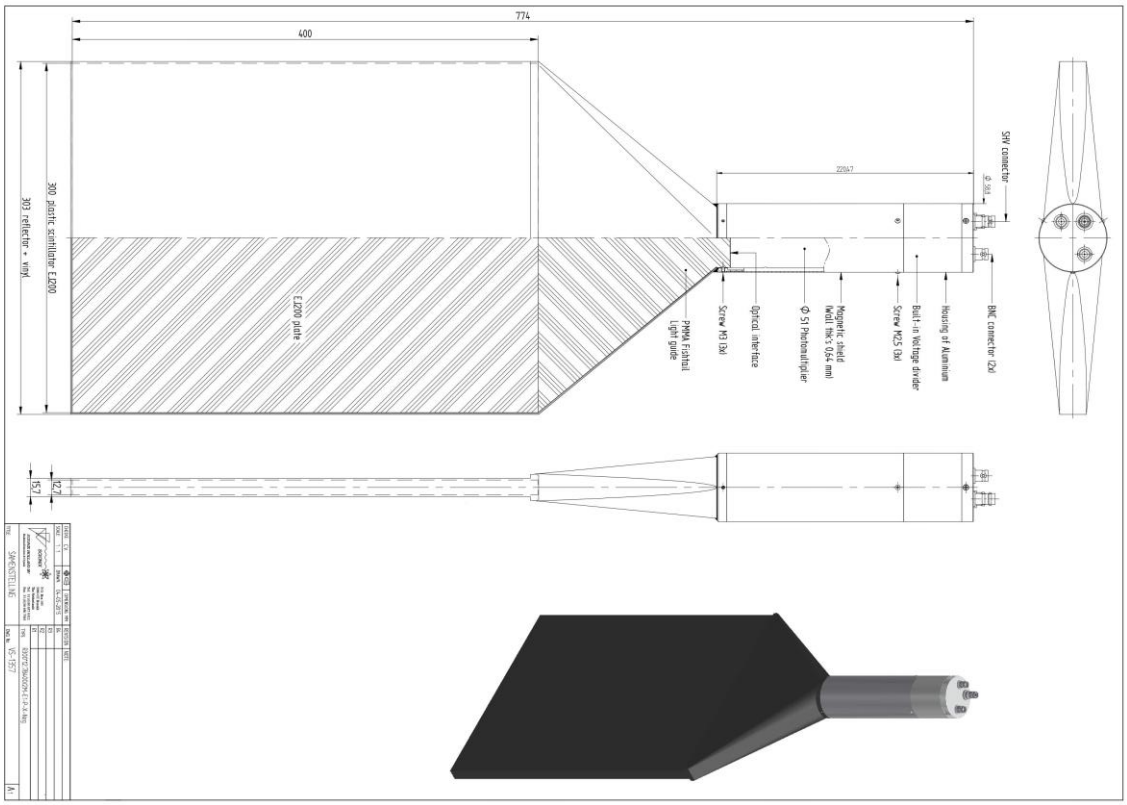

Figure 2. Technical drawing of a 12.7 mm thick EJ-200 plastic scintillator.

EJ-200 physical and scintillation constants	
Light output in % relative to anthracene	64
Scintillation efficiency, photons per 1 MeV e^-	10000
Wavelength of max. emission, nm	425
Rise time, ns	0.9
Decay time, ns	2.1
Pulse width, FWHM	2.5
Number of H atoms per cm^3	5.17×10^{22}
Number of C atoms per cm^3	4.69×10^{22}
Number of electrons per cm^3	3.33×10^{23}
Density, g/cm^3	1.023
Polymer base	polyvinyltoluene
Organic fluors, %	3

Table 1. Technical specifications of the EJ-200 plastic scintillators characterised in this work. Data are taken from [4].

Photomultiplier properties	
Active diameter, mm	46
Quantum efficiency at peak, %	30
Luminous sensitivity, $\mu A\ lm^{-1}$	70
Single electron rise time, ns	2
Single electron FWHM, ns	3
Multi electron rise time, ns	3
Multi electron FWHM, ns	4.5
Transit time, ns	45
Weight, g	160

Table 2. Properties of the PMT (9214B series produced by ET Enterprises) that was coupled to the EJ-200 scintillators. Data are taken from [5].

General light guide properties	
Specific gravity, ρ_{sample}/ρ_{H2O}	1.19
Refractive index, n_D (436 nm)	1.492
Refractive index, n_D (589 nm)	1.502
Softening point, °C	96
Number of H Atoms per cm^3	5.73×10^{22}
Number of C Atoms per cm^3	3.58×10^{22}
Number of O Atoms per cm^3	1.43×10^{22}
Number of Electrons per cm^3	3.86×10^{23}

Table 3. Properties of the light guide. Data are taken from [6], [7].

3 Data acquisition

The anode and dynode output of the PMT were directly connected to a DT5730B or DT5751 digitizer from CAEN. The 5730B digitizer has a resolution of 14 bits and a sampling rate of 500 MS/s on each channel [8]. The CAEN DT5751 digitizer samples the signal at a rate of 1 GS/s with a 10 bits resolution. Figure 3 shows a schematic representation of the full system.

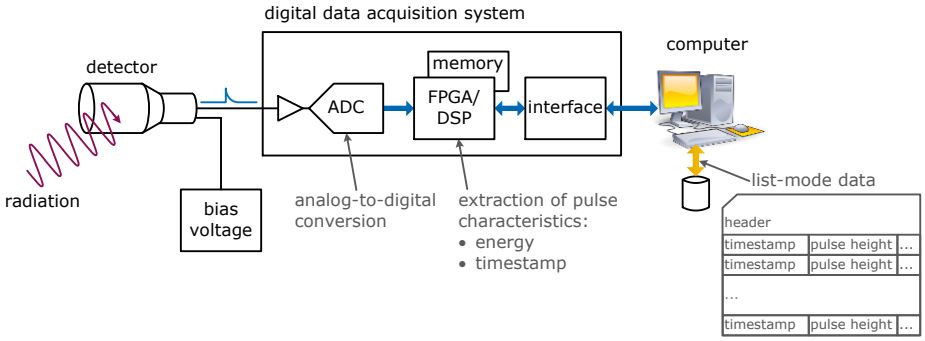

Figure 3. Digital data acquisition system acquiring data in list mode.

The data acquisition and pre-processing was executed by the digitizer and the associated firmware Digital Pulse Processing – Pulse Shape Discrimination (DPP-PSD). A detailed description of the acquisition algorithm can be found in [8]. An example of a detector signal together with the parameters used to analyse the signal is shown in Figure 4.

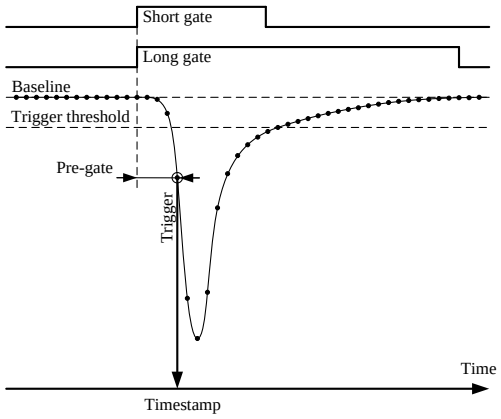

Figure 4. Representation of the signal acquisition logic in the DPP-PSD firmware of the CAEN module. Taken from [8].

A detected signal is sampled by an analogue-to-digital converter. The firmware calculates a baseline as a moving average of samples. When the sample value exceeds the baseline by the trigger threshold, the pulse is processed. All pulses below this trigger level are not processed. When the pulse is processed, its timestamp is kept, and two gates with different adjustable widths are opened. The gates open a certain time (pre-gate) before the trigger. The signal samples are integrated (summed) along the gate width, which results in two integrated charges, Q_s and Q_L for the short and long gate, respectively. The signal Q_L obtained with a gate length of 200 ns was used for the characterisation of the detectors.

The trigger time tag together with the integrated charges Q_s and Q_L are written into a binary output file. The binary list-mode output file is converted with ROOT to a root file. ROOT is an object-oriented framework for data analysis and visualisation written in C++ and developed by CERN. ROOT is used in this work to process the measured data files, generate histograms, make data selections, perform fitting, etc.[10].

4 Data analysis

To determine the light output function $f(E_{cp})$ and resolution function σ_L^2, for both electrons and protons a procedure similar as in [11] and [12] was applied. The measured response N_{exp} was compared with the theoretical one N_M using a weighted least squares fit procedure. The theoretical response is expressed as:

$$N_M(L) = C \int \int R_2(L, E_{cp}) R_1(E_{cp}, E) \cdot \Phi_E(E) \cdot dE_{cp}\, dE \tag{4.1}$$

For the analysis of the spectra obtained from gamma rays, the response R_1 was derived from Monte Carlo simulations using MCNP [13], while for the analysis of the spectra obtained from neutron measurements a simple rectangular distribution was supposed. The function R_2 was parameterised by a Gaussian distribution:

$$R_2(L, E_{cp}) = \frac{1}{\sqrt{2\pi\sigma_L^2}} \cdot e^{-\left(\frac{-\left(L - f(E_{cp})\right)^2}{2\sigma_L^2}\right)}, \tag{4.2}$$

where the light output function $f(E_{cp})$ depends on the energy of the charged particle E_{cp} and resolution function σ_L^2 on the light that is produced by the charged particle. Ideally $f(E_{cp})$ and σ_L^2 are directly proportional to the energy E_{cp}. Both the light output and resolution function are characteristic for each individual detector type and geometry [14], [15]. Light output functions have been extensively studied for a variety of scintillators of different type and size [15]-[20]. They strongly depend on the type of charged particle creating the light pulse [14], [17], [18].

To determine $f(E_{cp})$ and σ_L^2 for a particular E_{cp} from the experimental response to mono-energetic gamma or neutron beams a least squares adjustment can be applied in the high light output region. For the response to a mono-energetic gamma ray, this region is limited to the light output produced by the electrons with an energy around the Compton edge. For the response to neutrons this region corresponds to maximum light output which is delivered by protons with an energy that equals the incoming neutron energy. These protons result from a head-on elastic scattering on hydrogen. The parameters α and β link the observed amplitude and the resolution by:

$$f(E_{cp}) = \alpha E_{cp} \tag{4.3}$$

$$\sigma_L^2 = \beta f(E_{cp}). \tag{4.4}$$

The behaviour of α and β as a function of E_{cp} determines the functional forms of $f(E_{cp})$ and σ_L^2. A not constant α versus energy indicates a nonlinear energy deposition or a nonzero offset or both. If β is not constant it indicates that the variation of the energy deposition is not only based on statistical processes.

For the majority of scintillators, the light output produced by electrons L_e is a linear function of the electron energy in the energy range between 0.04 MeV and 1.6 MeV [21]-[23]. Therefore, the light output in channels is mostly transferred into an electron equivalent light output expressed in energy units based on experimental observed light output for electrons. At higher electron energies deviations from the linear dependence of the light output as a function of electron energy have been reported in references [20], [23], [24], [23]. The light output produced by charged particles, e.g. protons, heavier than an electron is known to be non-linear [16]. Various parametric formulae have been proposed to describe them, ranging from a semi-empirical approach based on the specific energy loss [17]-[20], [25]-[27] to full empirical analytical expressions as a

function of the charged particle energy [20], [28], [29]. The formula used by Tomanin et al. [12]:

$$f(E_{cp}) = E_{cp}\left(b_0 + \frac{b_1 E_{cp}}{1 + b_2 E_{cp}}\right), \tag{4.5}$$

is a modified version of the one used by Kornilov et al. [20]. The resolution function σ_L^2 can mostly be been parameterized by [14], [21], [30]:

$$\sigma_L^2 = c_0 + c_1 L + c_2 L^2. \tag{4.6}$$

This equation accounts for the independent contributions due to the electronic noise c_0, the statistical nature of the light production and amplification c_1, and the position-dependent light transmission from the scintillator to the photocathode c_2.

5 Determination of the response function

To characterize the EJ-200 plastic scintillation detectors, experiments in different radiation fields were performed. The response to gamma rays was determined by measurements with radionuclide sources. To determine the response to neutrons results from measurements with mono-energetic neutrons were combined with results from time-of-flight experiments. The response to muons was verified by background measurements, i.e. measurements without radionuclide sources or neutron beams.

5.1 Response functions for gamma-rays

5.1.1 Experimental conditions

Experimental response functions for γ-rays were obtained by measurements with a set of radionuclide sources. For these experiments the SFQ 538 scintillator (12.7 mm), the SFQ 540 (20.0 mm) and the SFQ 542 (25.0 mm) were used. The response to four radionuclide sources was determined. The characteristics of these sources are specified in Table 4. The sources were placed on the detector surface in the middle of the scintillator. The anode and last dynode signals from the PMT were connected to a CAEN DT5730B digital data acquisition system. The high voltage of the photomultipliers was set to -1700 V. The detectors were positioned vertically.

Fields	$T_{1/2}$ / y	A / kBq	E_γ / keV	E_C / keV
^{137}Cs	30.05 ± 0.08	81	662	477
^{208}Tl(from ^{232}Th)	(14.02 ± 0.06) × 10^9	4	2614	2381
^{241}AmBe	432.6 ± 0.6	1.5 × 10^6	4438	4201
^{238}PuC	87.74 ± 0.03	5.6 × 10^6	6130	5884

Table 4. Characteristics of the radionuclide used used to determine the response functions to gamma rays (half-life data taken from [31]).

5.1.2 Results

The experimental response functions obtained with the 25 mm thick EJ-200 detector using the Cs, Th and PuC source are shown in Figure 5, Figure 6 and Figure 7, respectively. These responses were derived from the dynode signal. The spectra were transferred into an energy scale based on the position of the Compton edge at E_C = 5884 keV derived from measurements with the PuC source. The experimental response functions were fitted in a region around the Compton edge with the theoretical distribution obtained from MCNP simulations, which were folded with a Gaussian response function as described in Section 4.

Around the Compton edge there is a good agreement between the experimental and theoretical response functions. For the ^{137}Cs source a good agreement is obtained down to the light output corresponding to the electronic threshold at 250 keV. For ^{232}Th, AmBe and PuC the experimental response in the low energy region is higher than the theoretical one. This is mainly due to the limitations of the theoretical response which was only simulated for the gamma ray with the highest energy emitted from the source.

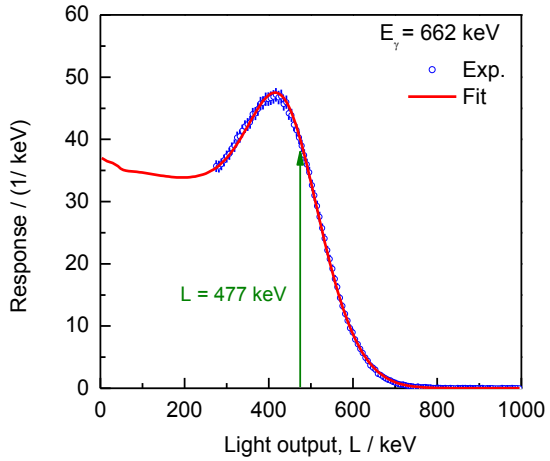

Figure 5. Experimental response function for a 25.0 mm thick EJ-200 plastic scintillator resulting from measurements with a ^{137}Cs source. The experimental response, derived from the dynode signal, is compared with the theoretical response. The arrow indicates the light output corresponding to the Compton edge at E_C = 477 keV.

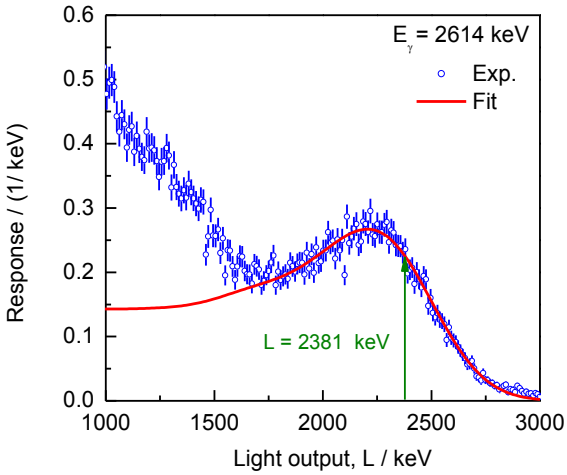

Figure 6. Experimental response function for a 25.0 mm thick EJ-200 plastic scintillator resulting from measurements with a ^{232}Th source. The experimental response, derived from the dynode signal, is compared with the theoretical response. The arrow indicates the light output corresponding to the Compton edge at E_C = 2381 keV.

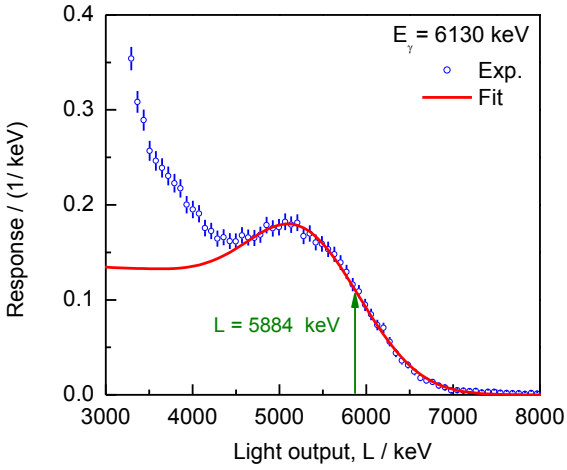

Figure 7. Experimental response function for a 25.0 mm thick EJ-200 plastic scintillator resulting from measurements with a PuC source. The experimental response, derived from the dynode signal, is compared with the theoretical response. The arrow indicates the light output corresponding to the Compton edge at E_C = 5884 keV.

From the result of the least squares adjustments the parameters α and β defined in Equation (4.3) and (4.4), respectively, were derived. The resulting specific light output α, derived from the last dynode and anode signal, are compared in Figure 8 as a function of electron energy. The results in Figure 8 illustrate that the light output derived from both the dynode and anode signal show a non-linearity as a function of electron energy. The linearity of the dynode signal improves with the thickness of the detector. This non-linear behaviour coincides with a substantial difference between the specific light output derived from the anode and last dynode. Since all light outputs were normalised to the Compton edge for the 6130 keV gamma ray from measurements with a PuC source, one does not expect a difference in specific light output derived from the anode and last dynode signal. For the transformation of observed light output in terms of amplitude into an energy scale the amplitude corresponding to the Compton edge at E_C = 5884 keV was used.

The non-linear dependence can be related to the performance of the PMT [32] and can be due to the applied bias high voltage. To study the effect of the bias voltage gamma response functions at voltages of -1700 V, -1770 V and -1820 V were determined for the SFQ 542 (25 mm) scintillator. Measurements were also carried out with an analogue data acquisition system. The obtained light output functions were compared with those from the measurements with the CAEN digitizers. Similar results were obtained, indicating that the data acquisition technique has no substantial impact on the results. Hence, the observed non-linearity as a function of applied bias voltage is most likely due to the PMT since the light production in the plastic scintillator is not affected by the bias voltage. It is known that this type of non-linearity is especially introduced at the last amplification stage in the PMT, resulting in a more linear response for the signal taken at the last dynode [32].

Table 5 reports the parameters for the light output produced by electrons based on Equation (4.5). The light output is derived from the signal taken from the last dynode. The parameters are given for the 12.7 mm, 20 mm and 25 mm thick EJ-200 scintillators. Uncertainties are only due to the propagation of counting statistics uncertainties.

	Parameters for L_{e^-} (12.7 mm)	Correlation matrix		
b_0	0.743 ± 0.007	1.00	-0.86	-0.76
b_1	$(8.30 \pm 1.00) \times 10^{-5}$		1.00	0.98
b_2	$(1.50 \pm 0.75) \times 10^{-4}$			1.00

	Parameters for L_{e^-} (20.0 mm)	Correlation matrix		
b_0	0.730 ± 0.006	1.00	-0.83	-0.72
b_1	$(5.90 \pm 1.00) \times 10^{-5}$		1.00	0.97
b_2	$(4.60 \pm 2.00) \times 10^{-5}$			1.00

	Parameters for L_{e^-} (25.0 mm)	Correlation matrix		
b_0	0.719 ± 0.005	1.00	-0.80	-0.70
b_1	$(5.75 \pm 0.85) \times 10^{-5}$		1.00	0.96
b_2	$(3.35 \pm 1.50) \times 10^{-5}$			1.00

Table 5. Parameters of the light output function of electrons based on equation (4.5). The parameters are given for a 12.7 mm, 20.0 mm and 25.0 mm thick EJ-200 scintillator purchased from SCIONIX. The uncertainties and correlation matrix were obtained by only propagating counting statistics uncertainties.

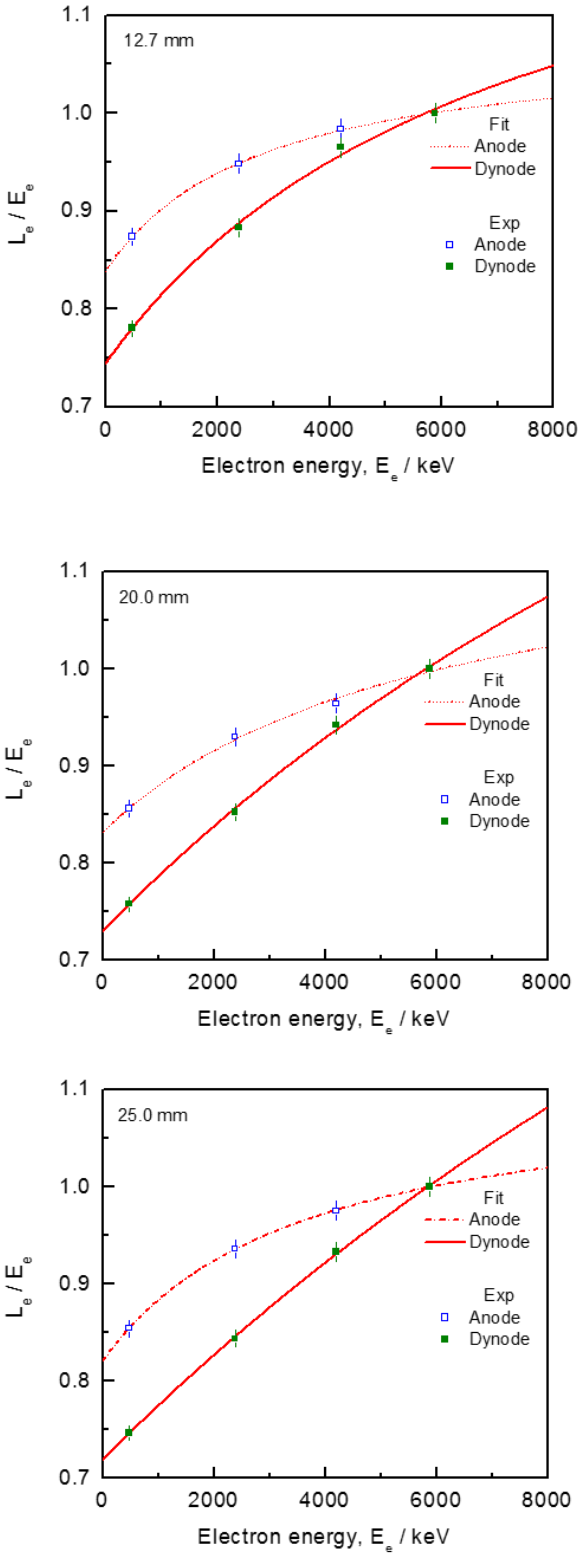

Figure 8. Specific light output for electrons as a function of electron energy for a 12.7 mm, 20.0 mm and 25.0 mm thick EJ-200 plastic scintillator purchased from SCIONNIX. The full line represents the result of a fit to the data using equation (4.5).

The relative resolution as a function of light output, which was derived from the parameters β is shown in Figure 9. The data are for a 12.7 mm, 20.0 mm and 25.0 mm EJ-200 scintillator. The full line represents the resolution based on equation (4.6). The parameters describing the full line in these figures have been determined from a fit of all data points, including the data obtained from the neutron measurements discussed in Section 5.2.

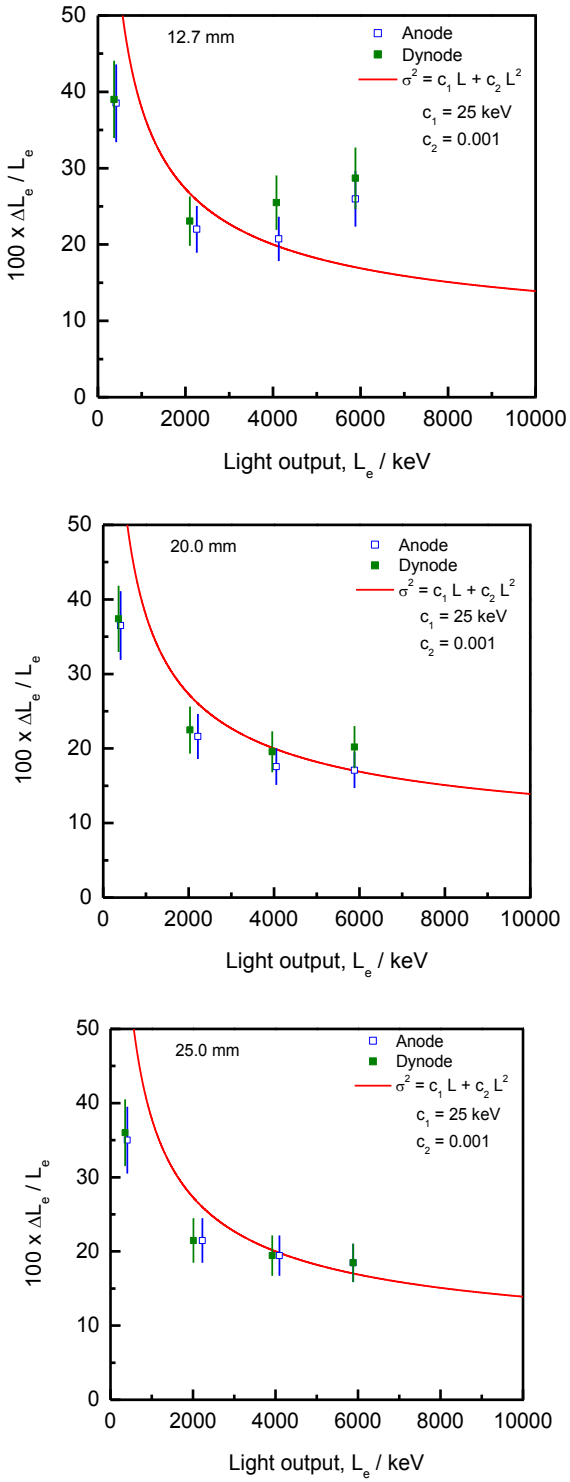

Figure 9. Relative resolution $\frac{\Delta L}{L}$ for a 12.7 mm, 20.0 mm and 25.0 mm thick EJ-200 scintillator purchased from SCIONIX. The resolution ΔL is expressed in FWHM and the relative resolution is given as a function of the electron light output L.

5.2 Response functions for neutrons

5.2.1 Experimental conditions

Response functions for neutrons were determined for the SFQ 538 (12.7 mm), SFQ 540 (20 mm) and SFQ 542 (25 mm) scintillators. Data were acquired with a CAEN DT5730B digitizer. The PMT bias voltages were adjusted to have the Compton edge due to the detection of a 662 keV gamma ray at approximately to the same amplitude. This resulted in voltages of -1715 V, -1760 V and -1756 V, respectively.

Measurements were performed at the Van de Graaff accelerators of the JRC Geel (B) and INFN Legnaro (I). At JRC Geel (B) the DPP-PSD control software provided by CAEN was used. At INFN Legnaro (I), the data throughput rate to enable fully digital time-of-flight measurements was too high for the DPP-PDS control software. Therefore, a software developed at JRC Geel (B) was applied. To convert the light output of the scintillator into an energy scale, measurements with a Cs radionuclide source were carried out. The amplitude spectra were transferred into energy based on the Compton edge position at $E_C = 5884\,\mathrm{keV}$. This position was derived from ^{137}Cs measurements and the ratio $L(E_{e^-} = 5884\,\mathrm{keV})/L(E_{e^-} = 477\,\mathrm{keV})$ resulting from the gamma calibration measurements.

Measurements with mono-energetic neutron beams were carried out at the 7 MV Van de Graaff accelerator of JRC Geel (B). The $d(d,n)\,^3He$ reaction was used in an energy range from 4.0 MeV to 6.5 MeV and the $t(d,n)\,^4He$ reaction in an energy range from 17.5 MeV to 19.0 MeV. The deuteron energies and corresponding neutron energies are reported in Table 6. Response functions were determined with the detectors placed at a 189 cm distance from the target and behind a 53 cm long collimator. All measurements were performed at 0° with respect to the direction of the charged particle beam. Figure 10 shows the experimental setup for the measurements with the SFQ 542 detector.

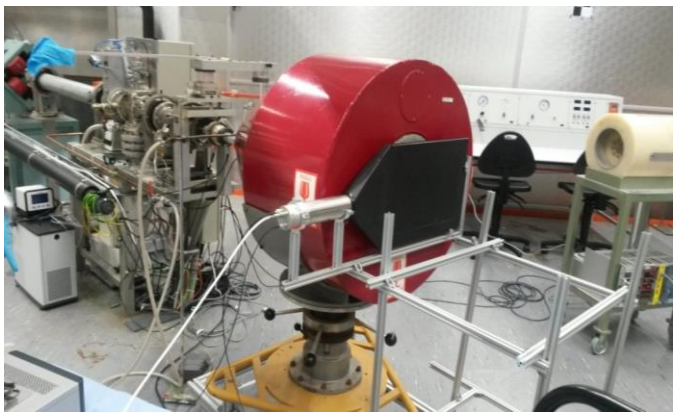

Figure 10. Experimental setup for the measurements at the VdG of the JRC Geel (B).

Nuclear reaction	Charged particle energy / keV	Neutron energy / keV	Target thickness / µg cm^{-2}	$\Delta E_N/E_N$ / %
d(d,n)^{3}He	1088	4000	1900	46.6
	1497	4500		26.6
	1932	5000		17.0
	2388	5500		12.1
	2861	6000		8.9
	3344	6500		6.8
t(d,n)^{4}He	1671	17500	2012	23.5
	1986	18000		17.5
	2328	18500		13.4
	2687	19000		10.5
^{7}Li(p,n)^{7}Be	4650	3000	13350	

Table 6. Properties of the proton and neutron beams for the measurements at the VdG facilities of the JRC Geel (B) and the INFN Legnaro (I).

The 7 MV Van de Graaff accelerator at INFN Legnaro (I) was operated in pulsed mode at a 600 kHz frequency. Protons were accelerated to an energy of 4.65 MeV. They were directed towards a 250 μm thick metallic Li target to produce neutrons via the ^{7}Li(n,p) reaction. The proton energy and the corresponding neutron energy are specified in Table 6. Properties of the proton and neutron beams for the measurements at the VdG facilities of the JRC Geel (B) and the INFN Legnaro (I). Experimental neutron response functions for a 25 mm thick EJ-200 plastic scintillator were obtained. Figure 11 shows the experimental setup at INFN Legnaro (I). A neutron collimator was positioned concentric with the proton beam between the target and neutron detector. The distance between the target and detector was 172.3 cm. A 51 cm long collimator was placed between the target and detector at 5.0 cm from the neutron producing target. The opening diameter of the collimator was 2.6 mm.

Figure 11. Experimental setup for neutron measurements at the INFN Legnaro (I).

An example of a time-of-flight (TOF) spectrum obtained with a 4.65 MeV pulsed proton beam is shown in Figure 12. The figure shows a sharp gamma flash peak at low TOF values, followed by a neutron peak. The neutron peak is followed by a tail, which is caused by neutrons with a lower energy. TOF cuts with a 1 ns TOF window were applied to extract response functions at given neutron energies. The corresponding neutron energy spread is much less than the energy resolution of the light output.

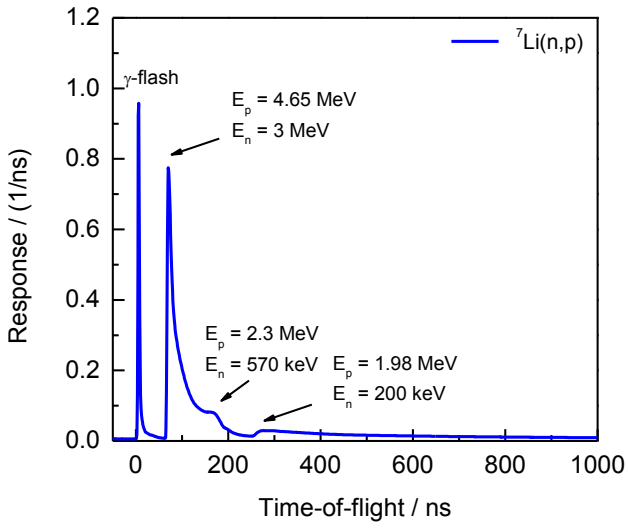

Figure 12. A time-of-flight spectrum resulting from measurement with a pulsed 4.65 MeV proton beam on a 250 μm thick solid Li-target.

5.2.2 Results

Experimental response functions for neutrons with an energy of 4.5 MeV are shown in Figure 13 and Figure 14 and for a neutron energy of 19 MeV in Figure 15.

The spectra were used to determine the specific light output and relative resolution for different proton energies by a fit in the region of a maximum transfer of neutron to proton energy. As mentioned before, for this analysis a rectangular distribution for the transfer of neutron to charged particle energy was supposed. The results of such a fit are shown in Figure 13, Figure 14 and Figure 15. These figures include the theoretical response taking into account a non-linear behaviour of the proton light output. They show, that in the region of maximum energy transfer there is a good agreement between the theoretical and experimental response. Evidently, to describe the response for light outputs below 1000 keV in Figure 13 and Figure 14 and below 12000 keV in Figure 15, a more accurate model for the transfer of neutron to charged particle energy is required. The model should include multiple interaction events and interactions with carbon accounting for the non-linear behaviour of the proton light output.

For low energy neutrons there is almost no difference between the response derived from the last dynode signal and the anode signal. On the other hand, there is a substantial difference between the response for a 19 MeV neutron beam derived from the last dynode and anode signal. The experimental response derived from the anode signal in the region of maximum energy transfer cannot be described based on a rectangular distribution folded with a Gaussian distribution. Apparently, also the experimental response for a 19 MeV neutron derived from the anode signal is not consistent with the theoretical one which includes the non-linear light output for protons. The results in Figure 15 reveal that this discrepancy is not due to the well-known non-linear behaviour of the light output for protons.

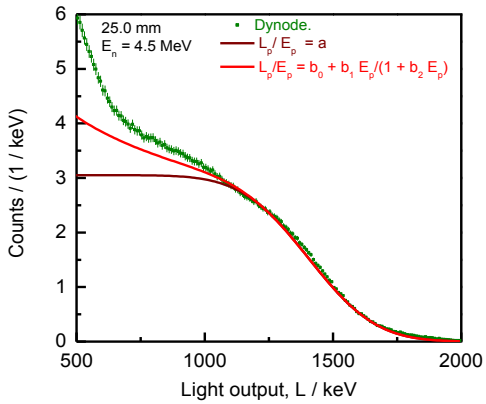

Figure 13. Experimental response function for a 4.5 MeV neutron beam. The response results from the last dynode signal of a 25 mm thick EJ-200 scintillator. The response function is fitted in the region of full transfer of neutron to proton energy with a theoretical response function based on two light output functions.

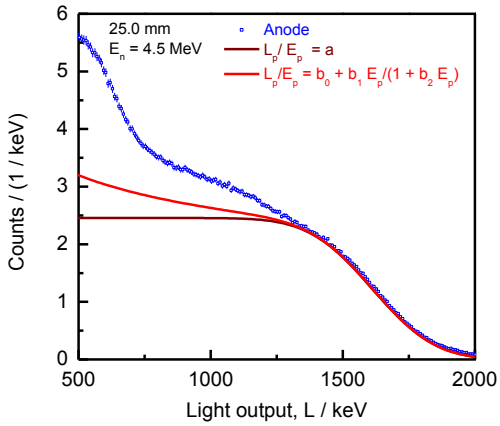

Figure 14. Experimental response function for a 4.5 MeV neutron beam. The response results from the anode signal of a 25 mm thick EJ-200 scintillator. The response function is fitted in the region of full transfer of neutron to proton energy with a theoretical response function based on two light output functions.

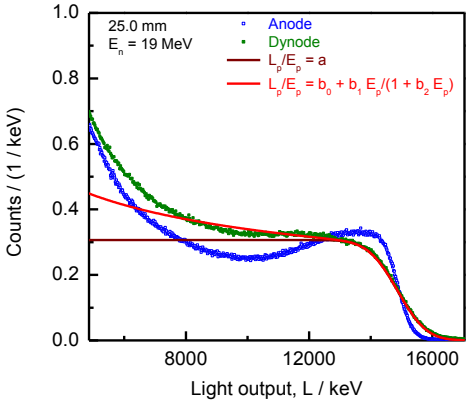

Figure 15. Experimental response function for a 19 MeV neutron beam. The response from the last dynode and anode signal of a 25 mm thick EJ-200 scintillator are compared. The response function is fitted in the region of full transfer of neutron to proton energy with a theoretical response function based on two light output functions.

From the results of the least squares adjustment the specific light output and relative resolution was derived for different proton energies. The specific light output as a function of proton energy for the 25 mm thick EJ-200 detector is shown in Figure 16. One observes a difference between the results obtained from the anode and last dynode signal. Hence, part of the non-linearity is due to the treatment of the signal and not due to the transfer of charged particle energy into light. The non-linearity observed for protons is mainly due to the light production process. The results in Figure 16 also show that the light output for protons is about a factor 3 smaller compared to the one for electrons.

The light output function was fitted using the analytical expression in Equation (4.5). The result of the least squares adjustments are shown in Figure 16. The parameters resulting from a fit to the data for the 25 mm thick detector are given in Table 7. Uncertainties are only due to the propagation of counting statistics uncertainties.

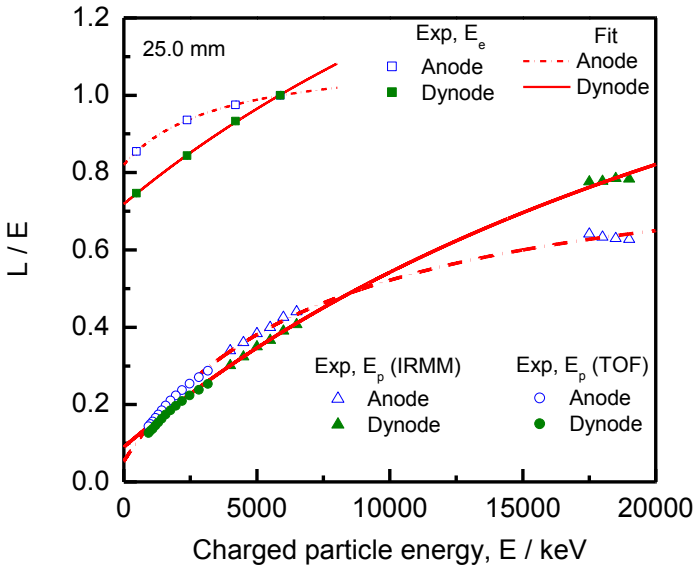

Figure 16. Specific light output for electrons and protons for a 25 mm thick EJ-200 scintillation detector. The data derived from the response functions for gamma rays are represented by □, for neutrons from the VdG data of the JRC Geel (B) by Δ and for neutrons from the time-of-flight data at the INFN Legnaro (I) by ○ . The full and dashed lines are the result of a fit using equation (4.5).

	Parameters for L_p (25.0 mm)	Correlation matrix		
b_0	0.090 ± 0.015	1.00	-0.99	-0.98
b_1	$(5.92 \pm 0.05) \times 10^{-5}$		1.00	0.99
b_2	$(3.10 \pm 0.06) \times 10^{-5}$			1.00

Table 7. Parameters for the proton light output function L_p based on equation (4.5) for a 25.0 mm thick EJ-200 detector.

The relative resolution $\frac{\Delta L}{L}$ of the 25 mm thick detector as a function of the light output L is shown in Figure 17. In this figure the data obtained from measurements with gamma sources and neutron beams are shown. The figure confirms that the resolution as a function of light output is not strongly dependent on the particle type. The data were fitted using Equation (4.5). The parameters resulting from the fit are $c_1 = 25\,\mathrm{keV}$, $c_2 = 0.001$ and c_0 can be neglected.

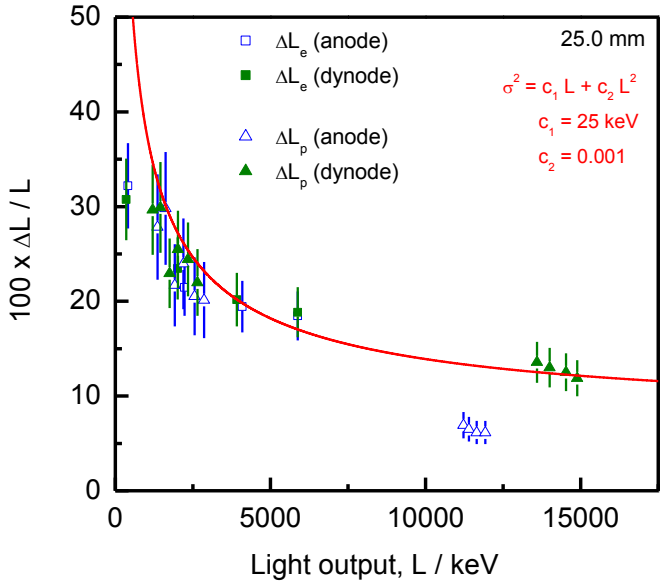

Figure 17. The relative resolution $\frac{\Delta L}{L}$ as a function of the light output L for the SFQ 542 (25.0 mm) detector. The data points are obtained from measurements with gamma-ray sources and from neutron beam measurements. The square (□) represents the data resulting from the gamma ray measurements and the triangle (Δ) represents the data derived from the response functions for neutrons. The full line is the last squares fit using the gamma ray and the neutron data.

5.3 Response functions for muons

5.3.1 Experimental conditions

Experimental response functions for muons were derived from measurements without any radiation source. They were determined with the scintillator placed vertically and horizontally. In addition, measurements with stacked detectors were carried out. Before running the background measurements, the high voltage for each detector was adjusted to have the Compton edge at 478 keV at the same amplitude in the spectrum obtained from measurements with a ^{137}Cs source. The resulting voltages are listed in Table 8. After matching the gain of the PMTs, the ^{137}Cs source was removed and three consecutive background measurements were started for a time of almost 3 days. The amplitude spectra were transferred into an energy scale based on the position of the Compton edge at E_c = 5884 keV. This position was derived from the results of the ^{137}Cs measurements together with the ratio $L(E_{e^-} = 5884\,\mathrm{keV})/L(E_{e^-} = 477\,\mathrm{keV})$ resulting from the gamma calibration measurements.

Detector	Thickness / mm	HV (after matching) / V	dE (horizontal) / MeV
SFQ537	12.7	-1350	2.6
SFQ539	20	-1826	4.1
SFQ541	25	-1515	5.1

Table 8. Applied high voltage for the three detectors.

5.3.2 Results

Figure 18 shows a spectrum resulting from background measurements with a 25 mm EJ-200 detector. In the natural background, apart from muons also gamma rays from the decay of ^{40}K and ^{208}Tl are present. They have an energy of 1460 keV and 2614 keV, respectively. The corresponding Compton edges can be clearly observed at 1243 keV and 2381 keV. ^{208}Tl is one of the decay products in the ^{232}Th series [33], and is the highest energy gamma ray emitter that can be expected in a normal background. No difference in response to this gamma ray background between a horizontally and vertically oriented detector is observed in Figure 18.

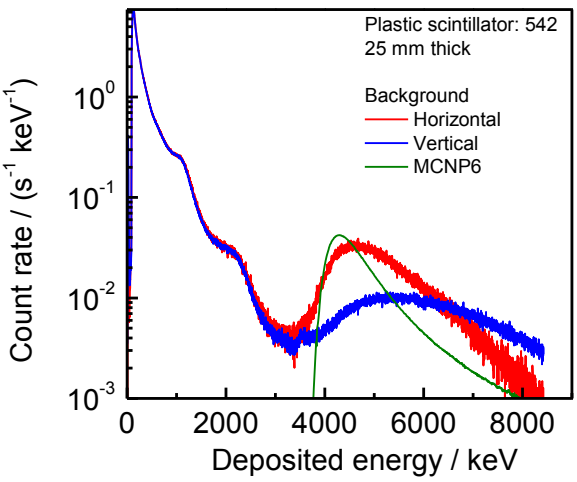

Figure 18. Response of a 25 mm detector to background radiation. The results for the detector placed horizontally and vertically are compared. The Compton edges of the gamma rays at 1.2 MeV and 2.4 MeV due to the decay of ^{40}K and ^{208}Tl, respectively, can be clearly observed. The peak at 5 MeV corresponds to the energy deposited by muons passing through the horizontally paced detector. The muon peak for the vertically placed detector is broader and appears at a higher energy. The thin line is the result of Monte Carlo simulations for the energy deposited by muons in the horizontally placed detector.

However, for the response to muons the orientation of the detector plays a role. The intensity of the muon background follows a $cos^2\theta$ distribution, with the angle θ taken with respect to the normal on the surface of the horizontally oriented detector. A clearly distinguishable peak in the region between 4 MeV and 5 MeV can be observed. This peak results from muons that pass completely through the horizontally oriented detector. When the detector is positioned vertically, the peak intensity is lower as the area of the detector appears to be smaller from the direction where the muons enter. The peak appears at a higher energy, because muons can now travel a larger distance inside the detector and deposit more energy. At last, the peak is also broader for the vertical detector, since due to the geometry and the muon angular dependence, a larger spread in their path length in the detector is expected. The response of the horizontal detector was also simulated my means of MCNP, and shown in the figure by the thin line. The simulated response was not folded with the resolution function, but it can be observed that its position and shape correspond well with the observed response. This suggests that the light output for muons is similar to the one for electrons.

Figure 19 compares the responses of the three detectors with different thickness, oriented horizontally and vertically. The measurement time was the same for the six measurements. As in the previous figure, the natural gamma background can be observed at energies up to about 3 MeV. Obviously, the absolute contribution of the natural gamma background depends on the thickness of the detector, but not on its orientation. From the peaks corresponding to the detection of muons a specific energy loss of about 2 MeV cm^{-1} can be derived.

For the detectors with a thickness of 20 mm and 25 mm and oriented horizontally, the Compton edges of gamma rays resulting from the decay of ^{40}K and ^{208}Tl are clearly visible. For the 20.0 mm and 25.0 mm thick detector, the background due to gamma-rays is well-separated from the peak caused by the detection of muons that traverse the detector. However, for the 12.7 mm thick detector, the energy deposited by the muon is about 2.5 MeV, which overlaps with the Compton edge of a 2.6 MeV gamma ray. For that detector only the Compton edge of the gamma ray due to the decay of ^{40}K is visible. Hence, energy discrimination between the background from gamma-rays and muons is straightforward for the thicker horizontal detectors, but impossible for the thin detector.

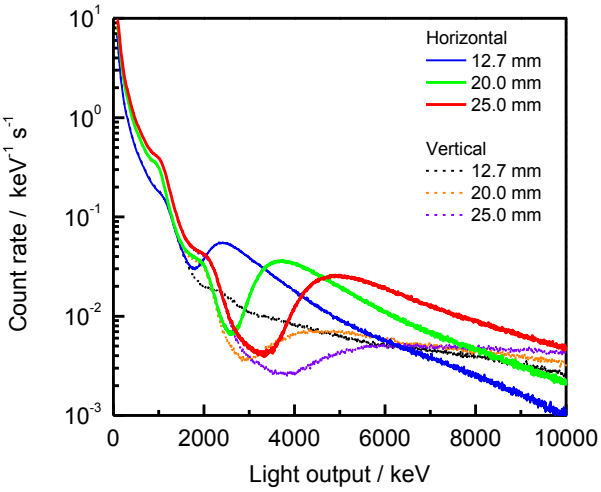

Figure 19. Results of background measurements with EJ-200 detectors with different thicknesses oriented horizontally and vertically. A difference in the shape of the muon peaks can be observed.

Additional measurements were performed with the three detectors oriented horizontally, but stacked. The vertical distance between the detectors was 7 cm. The thinnest detector (12.7 mm) was placed on top. The 20 mm detector was in the middle and the thickest one (25 mm) was at the bottom of the stack. The results are shown in Figure 20. Obviously for the detector on top of the stack, there is no difference in response. For the middle detector and the one placed at the bottom of the stack, the response is

slightly lower for energies up to about 5.5 MeV for the middle detector and about 9 MeV for the bottom detector. Above these energies, more muons are observed for the detectors in the middle and the bottom of the stack.

This observation can be understood. As discussed earlier, muons either pass through the detector while they deposit an energy of 2 MeV cm^{-1} along their track, or they come to a full stop, after which they decay into an electron, a neutrino and an antineutrino. The 105.7 MeV c^{-2} rest mass of the muon is then shared as kinetic energy between the three particles. The electron will be absorbed in the detector and deposit its energy, but the two neutrinos will escape without being detected. The absorbed energy in the detector is higher when the muon decays than when the muon passes through the detector without being stopped. Muons that have passed already one or two detectors have lost part of their energy and are more likely to be stopped in the remaining detectors of the stack, causing a slightly higher response at higher energies, and a lower response at energies lower than 5.5 MeV and 9 MeV, respectively.

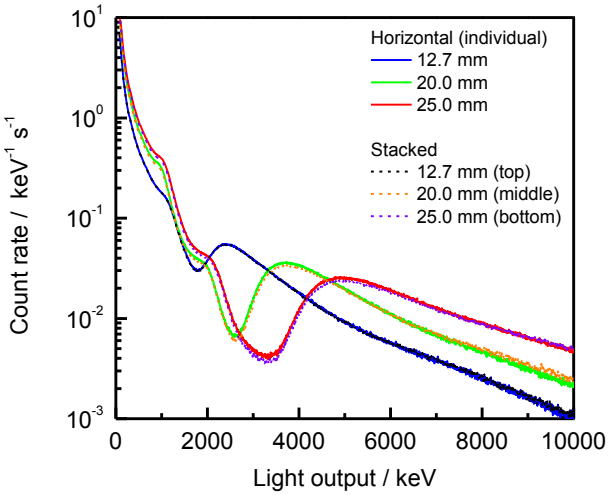

Figure 20. Results from background measurements, with the detectors oriented horizontally, both stacked and unstacked.

6 Muon coincidence detection

The final application aims at developing a veto logic that disables a neutron waste measurement system when a cosmic muon is detected. As discussed in section 4.3, this can already be done by an energy discrimination between background gamma rays and muons. A more effective veto system can be realised by stacking detectors and considering in addition to an energy discrimination also coincident events.

To investigate the effect of coincident events, measurements were carried out with the 20 mm placed on top of the 25 mm detector. Since the muon travels at relativistic speed, the difference in time of detection of the muon in the two detectors will be very small. This is illustrated in Figure 21, which represents the time-of-flight spectrum in which the start signal is taken from the detection of an event in the top detector and stop of the bottom detector. The timestamp of the stop signal was delayed by 100 ns to allow visualisation of the complete time-of-flight histogram. The resolution of the time stamps is mainly due to the 1 ns accuracy of the digitizer.

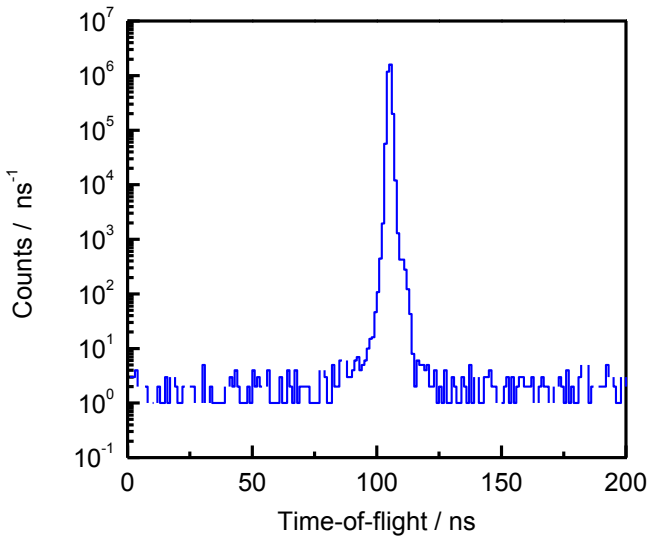

Figure 21. Time-of-flight histogram resulting from the difference in time of detection of a muon event in the top and bottom detector.

The time-of-flight spectrum shows a pronounced peak centred at about 100 ns due to the detection of coincident muons and a baseline due to random coincidences. From these findings, a criterion based on deposited energy and time-of-flight can be established. A criterion for accepting an event as a muon could be:

- the energy deposited in the top detector (20 mm) is larger than 2600 keV, AND
- the energy deposited in the bottom detector (25 mm) is larger than 3300 keV, AND
- time difference between 90 and 110 ns (after applying a 100 ns time shift).

In the final application, the threshold energies will have to be optimised as a function of the selected thickness for the detectors.

The effectiveness of applying the coincidence requirement was demonstrated by constructing the energy histogram for events in the top detector that cause a coincident detection in the bottom detector (timestamp difference between 90 and 110 ns). Figure 22 shows such a histogram, together with the histogram of all the events in the top detector.

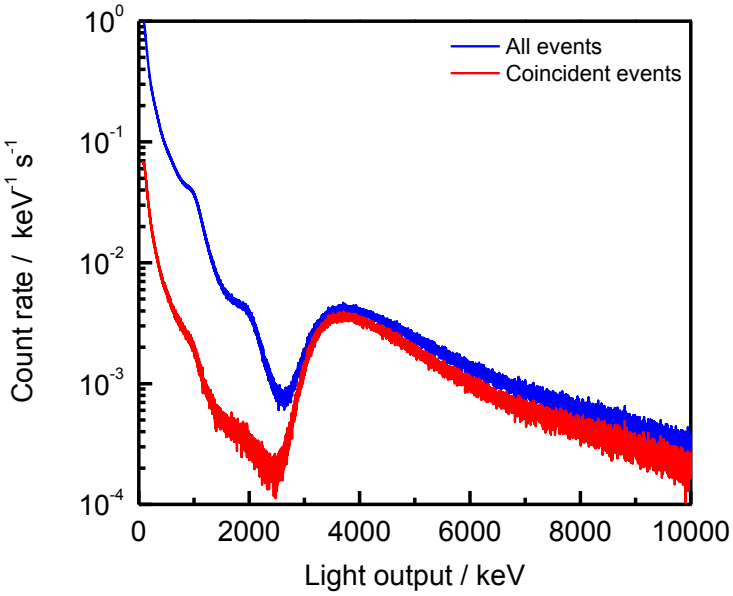

Figure 22. Demonstration of the effectiveness of the coincidence requirement when two detectors are stacked.

Independent of the energy, the number of events that are in coincidence is only 11% (see Table 9). However, these are practically all muons. If we add the requirement on the energy, one notices that 77% of the muons that travel through the top detector are also detected in the second detector.

Energy / MeV	Count rate of events in top detector / s^{-1}	Count rate of events in top detector that are in coincidence with bottom detector / s^{-1}	Ratio (coincident/all) / %
E < 2600	272.0	18.3	7
E ≥ 2600	18.1	13.9	77
Total	290.1	32.2	11

Table 9. Results of the coincidence measurements.

7 Summary and conclusions

A set of rectangular EJ-200 plastic scintillation detectors with different thicknesses were characterised for their response to gamma rays, neutrons and muons. The main objective was to demonstrate their use as veto detector to reduce the impact of muon background for waste characterisation measurements based on the detection of neutrons.

Commercial available detectors were calibrated for gamma ray energies ranging from 0.6 MeV to 6 MeV. The results for the gamma ray measurements show that there is a difference between the light output of the dynode and anode and a light output that is non-linear as a function of electron energy. The difference between results obtained from the last dynode and anode signal increases with increasing bias supply. Evidently the observed non-linearity is mainly due to a not optimised combination of PMT, voltage divider and recommended high voltage of the commercially available systems.

Neutron response functions were determined in an energy range from 4.0 MeV to 6.5 MeV and from 17.5 MeV to 19.0 MeV at the JRC Geel (B) Van de Graaff accelerator. Time-of-flight measurements were carried out at the Van de Graaff accelerator of the INFN Legnaro (I). The results of these measurements confirm that there is strong difference between response functions derived from the last dynode and the anode. Since the scintillators are not used as spectrometers, the performance of the scintillators as veto detectors will not be influenced by the observed non-linearities.

From the response functions for gamma rays and neutrons, light output and resolution functions for protons and electrons were derived. They were parameterised with analytical functions and the free parameters were obtained from a least squares adjustment to the data. It was shown that the light output for protons is about a factor 3 less compared to the one for electrons. The resolution as a function of light output does not depend on the charged particle type creating the light.

From the results of the background measurements it was concluded that the specific energy loss for muons in a EJ-200 plastic scintillator is about 2 MeV cm^{-1}. Using a scintillator with a minimum thickness of 20 mm a signal caused by the detection of a muon can be separated from 2614 keV gamma rays from ^{208}Tl, which are always present as a natural background component. The muon peak is better pronounced in horizontally oriented detectors compared to vertical ones.

For detectors that are stacked, signals caused by the detection of muons can also be identified based on a coincidence pattern. Hence, requirements on such a coincidence pattern together with requirements on the light production are effective as parameters for the veto system to be designed.

Acknowledgements

The experiments at the Van de Graaff accelerator of the JRC at Geel (Belgium) were supported by the 327-ARI-ET project (EUFRAT) of the JRC. We are grateful to the technical staff of the CN accelerator of the INFN Legnaro (I) and the Van de Graaff accelerator of the JRC Geel (B). FS acknowledges the financial support of the EURATOM Fission 7th Framework Programme's project GENTLE (grant number 323304) for the experiments at the VdG facility of JRC Geel (Belgium).

References

[1] W. Hage and D.M. Cifarelli, On the factorial moments of the neutron multiplicity distribution of fission cascades. Nuclear Instruments and Methods in Physics Research Section A 236 (1985) 165 - 177.

[2] D.M. Cifarelli and W. Hage, Correalation Analysis with Neutron Count Distributions in Randomly or Signal Triggered Time Intervals for Assays of Special Fissile Materials. Nuclear Science and Engineering 89 (1985) 159 - 176.

[3] D.M. Cifarelli and W. Hage, Models for a three-parameter analysis of neutron signal correlation measurements for fissile material assay. Nuclear Instruments and Methods 251 (1986) 550 - 563

[4] C. Maxwell, EJ-200 Plastic Scintillator data sheet. Sweetwater : Eljen Technology, 2010.

[5] ET Enterprises. 9214B series data sheet. Uxbridge : ET Enterprises Limited, 210.

[6] G. Knoll, Radiation Detection and Measurement. Michigan : John Wiley & Sons, 1989.

[7] C. Maxwell, Light Guides data sheet. Sweetwater : Eljen Technology, 2010.

[8] CAEN. Electronic Instrumentation DT5730.

[9] CAEN. Electronic Instrumentation. User Manual UM2580 DPP-PSD Digital Pulse Processing for Pulse Shape Discrimination. [Online] CAEN, 2015. [Cited: 11 December 2015.] http://www.caen.it/csite/CaenProd.jsp?parent=39&idmod=770.

[10] R. Brun and F. Rademakers, ROOT - An Object Oriented Data Analysis Framework. Nuclear Instruments & Methods in Physics Research Section A 389 (1996) 81 - 86.

[11] M. Weyrauch, A. Casnati, P. Schillebeeckx and M. Clapham, Use of ^{4}He-filled proportional counters as neutron spectrometers. Nuclear Instruments and Methods in Physics Research Section A 403 (1998) 442 – 454.

[12] A. Tomanin, J. Paepen, P. Schillebeeckx, R. Wynants, R. Nolte and A. Lavietes, Characterization of a cubic EJ-309 liquid scintillator detector. Nuclear Instruments and Methods in Physics Research Section A 756 (2015) 45 – 54.

[13] X-5 Monte Carlo Team. A General Monte Carlo N-Particle Transport Code, Version 5. Los Alamos : Los Alamos National Laboratory, 2003.

[14] H. Klein and S. Neumann, Neutron and photon spectrometry with liquid scintillation detectors in mixed fields. Nuclear Instruments and Methods in Physics Research Section A 476 (2002) 132 – 142.

[15] D. Schmidt, B. Asselineau, R. Böttger, H. Klein, L. Lebreton, S. Neumann, R. Nolte, and G. Pichnot, Nuclear Instruments and Methods in Physics Research Section A 476 (2002) 186 - 189.

[16] V.V. Verbinski, W. Burrus, T.A. Love, W. Zobel, N.W. Hill, and R. Textor, Calibration of an organic scintillator for neutron spectrometry. Nuclear Instruments and Methods in Physics Research Section 65 (1968) 8 - 25.

[17] R. Batchelor, W.B. Gilboy, J.B. Paker and J.H. Towle, The response of organic scintillators to fast neutrons. Nuclear Instruments and Methods in Physics Research Section 13 (1961) 70 - 82.

[18] R.L. Craun and D. L. Smith, Analysis of response data for several organic scintillators. Nuclear Instruments and Methods in Physics Research Section 80 (1970) 239 - 244.

[19] S. Mouatassim, G. Costa, G. Guillaume, B. Heusch, A. Huck and M. Moszyński, The light yield response of NE213 organic scintillators to charged particles resulting

from neutron interactions. Nuclear Instruments and Methods in Physics Research Section A 359 (1995) 530 – 536.

[20] N.V. Kornilov, I. Fabry, S. Oberstedt and F.-J. Hambsch, Total characterization of neutron detectors with a ^{252}Cf source and a new light output determination. Nuclear Instruments and Methods in Physics Research Section A 599 (2009) 226 – 233.

[21] G. Dietze, Energy calibration of NE-213 scintillation counters by gamma rays. IEEE Transactions on Nuclear Science NS-26 (1979) 398 – 402.

[22] G. Dietze and H. Klein, Gamma-calibration of NE 213 scintillation counters. Nuclear Instruments and Methods in Physics Research Section 193 (1982) 549 – 556. 193.

[23] T. Novotny, L. Buermann, S. Guldbakke and H. Klein, Response of NE213 liquid scintillation detectors to high-energy photons (7 MeV < Eγ < 20 MeV). Nuclear Instruments and Methods in Physics Research Section A 400 (1997) 356 – 366.

[24] L. Büermann, S. Ding, S. Guldbakke, H. Klein, T. Novotny and M. Tichy, Response of NE213 liquid scintillation detectors to high-energy photons (Eγ > 3 MeV). Nuclear Instruments and Methods in Physics Research Section A 332 (1993) 483 – 492.

[25] J. Birks, The Therory and Practice of Scintillation Counting. Oxford: Pergamon Press, 1964.

[26] C. N. Chou, Physical Review 87 (1952) 904.

[27] G. T. Wright, Physical Review 91 (1953) 1282.

[28] R. Madey, F.M. Watermann, A.R. Baldwin, J.N. Knudsen, J.D. Carlson and J. Rapaport, The response of NE-228A, NE-228, NE-224, and NE-102 scintillators to protons from 2.43 to 19.55 MeV. Nuclear Instruments and Methods in Physics Research Section 151 (1978) 445 – 450.

[29] W. Tornow, W. Arnold, J. Herdtweck and G. Mertens, Measurement of the response of the deuterated scintillators NE 232 and NE 230 to protons and deuterons. Nuclear Instruments and Methods in Physics Research Section A 244 (1986) 477 – 482.

[30] H. Schölermann and H. Klein, Optimizing the energy resolution of scintillation counters at high energies. Nuclear Instruments and Methods in Physics Research Section 169 (1980) 25 - 31.

[31] A. Arinc and E. Browne. Recommended Data. Laboratoire National Henri Becquerel. [Online] http://www.nucleide.org/DDEP_WG/DDEPdata.htm.

[32] S. Flyckt and C. Marmonier, Photomultiplier tubes - Principles and Applications. Brive : Photonis, 2002.

[33] Decay Chains. Nuclear Forensic Search Project. [Online] UC Berkeley research team. [Cited: 25 1 2016.] http://metadata.berkeley.edu/nuclear-forensics/Decay%20Chains.html.

List of abbreviations and definitions

DPP-PSD	Digital Pulse Processing – Pulse Shape Discrimination
FWHM	Full Width at Half Maximum
MCNP	general-purpose Monte Carlo N-Particle code
PMT	Photomultiplier Tube
VdG	Van de Graaff

List of figures

List of tables

LA-NA-27930-EN-N

JRC Mission

As the Commission's in-house science service, the Joint Research Centre's mission is to provide EU policies with independent, evidence-based scientific and technical support throughout the whole policy cycle.

Working in close cooperation with policy Directorates-General, the JRC addresses key societal challenges while stimulating innovation through developing new methods, tools and standards, and sharing its know-how with the Member States, the scientific community and international partners.

Serving society
Stimulating innovation
Supporting legislation

doi: 10.2787/810820

ISBN 978-92-79-58436-7